Development of Cooling Systems for Nuclear Fusion Components

Ricardo Tavares Rego

ricardorego@tecnico.ulisboa.pt

Instituto Superior Técnico, Universidade de Lisboa, Portugal

November 2017

Abstract

This work presents a study on the development of a cooling system for the launcher and receiver mirrors of the International Thermonuclear Experimental Reactor (ITER) Collective Thomson Scattering (CTS) system that is used for plasma diagnostics. It is motivated by the fact that these stainless steel 316L(N)-IG (SS 316L(N)-IG) mirrors are subjected to high thermal loads, e.g., neutron fluxes, that lead to maximum temperatures of the mirrors above the required operational temperature 450^0C. Hence, it is necessary to develop a cooling system capable of maintaining the maximum temperatures of the mirrors bellow 450^0C, while complying with the CTS and nuclear fusion requirements. Hence, Computer Aided Design (CAD) models of the mirrors with different cooling channel geometries, considering parallel and series fluid flow configurations, and different mass flow rates are developed. Besides SS 316L(N)-IG, tungsten (with an operational temperature of 1210^0C) and copper (with an operational temperature of 87^0C) are also considered for the mirrors and they present relative higher thermal diffusivity. Steady state and transient thermal Finite Element Analysis (FEA) are conducted for the assessment of the feasible solutions. The results obtained are conclusive, i.e., the cooling requirements are verified and with one of the proposed configurations it is possible to decrease the maximum temperatures of the SS 316L(N)-IG launcher and receiver mirrors from $\sim 2306^0C$ and $\sim 1064^0C$ to $\sim 381^0C$ and $\sim 240^0C$ which, corresponds to a maximum temperature decrease of 83.5% and 89.5%, respectively. Additionally, one concludes that: i) the use of copper for the mirrors is not viable as the minimum maximum temperature obtained is $\sim 105^0C$ which, is above the operational temperature of copper (87^0C) and; ii) on the other hand, the use of tungsten for the mirrors is a viable solution as one obtains a minimum maximum temperature of $\sim 151^0C$ which is below the operational temperature of tungsten (1210^0C). Even though tungsten seems to be a more adequate material for the mirrors as it presents lower maximum temperatures, the manufacturing processes of tungsten mirrors with cooling channel geometries should be further contemplated in future works.

Keywords: ITER, CTS, Cooling, Nuclear Fusion, Finite Element Analysis, Thermal Analysis

1. Introduction

Nowadays, energy harvesting management is an important and transversal topic among many areas as there are finite resources from which energy can be obtained.

Nuclear fusion energy is a clean energy solution that can occur in a tokamak which, is a system that confines plasma in a toroidal form, using magnetic fields [1].

The ITER tokamak, see Figure 1 taken from [2], is expected to be the first capable of producing energy with an efficiency > 1, actually ~10.

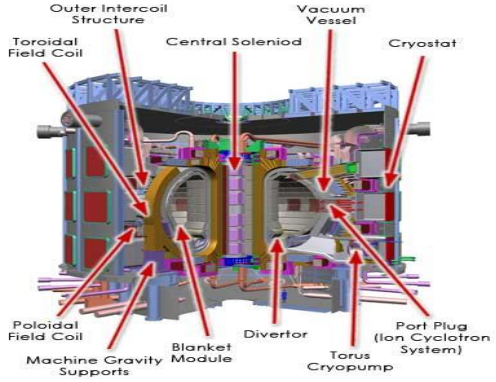

Figure 1 - Cutaway of the ITER Tokamak with the main components illustrated [2].

ITER is expected to have approximately fifty individual measurement systems for plasma diagnostic data, control aid, evaluation and performance optimization.

Of those, the CTS is an optical diagnostics system with the main function of measuring plasma temperature profiles and density [3].

Thomson scattering is the basic principle of the CTS system and it is an elastic dispersion of radiation by photons of uncharged particles and is basically the minimum energy limit of Compton scattering [4].

The ITER CTS system, see Figure 2, is equipped with a microwave source (60 GHz, 1.0 MW gyrotron), transmission lines, mirrors to reflect the incident beam, waveguides, a mm-wave detector system and electronic data acquisition and processing components, [3].

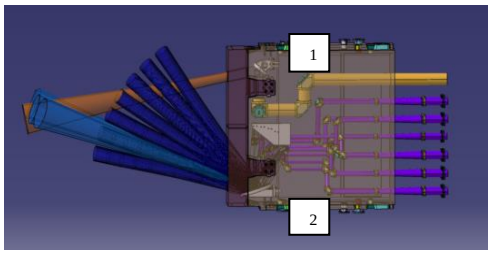

Figure 2 - ITER CTS system and launcher (1) and receiver (2) mirrors location, [3].

This work presents a study on the development of a cooling system for the ITER CTS launcher and receiver mirrors, that reflects the microwave beam into the plasma and that receives and guides the CTS signal into the waveguides, respectively.

This work is motivated by the fact that these SS 316L(N)-IG mirrors, which are in a vacuum environment and subjected to thermal loads that arise from: direct plasma thermal radiation; neutron fluxes from the nuclear fusion reaction; stray radiation from the surroundings and; the microwave launcher and receiver beams, do not survive operation as the maximum temperatures exceed the operational temperature of $450°C$.

Hence, it is necessary to develop a cooling system that can maintain the temperatures of the mirrors at an operational temperature $< 450°C$ while compiling with the CTS system requirements, e.g., inlet cooling fluid flow rate, and nuclear fusion requirements, e.g., the cooling fluid shall be water.

The first part of this study consists on the development of the CAD models of the two mirrors and for each mirror are developed ten different cooling channel geometries.

The second part of this study consists on the FE discretization and thermal FEA of the different mirror cooling configurations. FEA of the cooling channels geometries, implemented in the launcher and receiver mirrors are conducted. It is considered that, if necessary, tungsten and copper may also be considered as alternative materials for the mirrors. Afterwards, a transient thermal FEA of the most adequate combination material/cooling channel geometry for each mirror is conducted considering that ITER is expected to work in $400\ s$ pulses, with a dwell time of $1400\ s$ between pulses. To finalize, a steady state fluid flow thermal analysis is performed to verify the pressure drop and the convection coefficient used in the analyses.

The results obtained are conclusive, i.e., the cooling requirements are verified and with one of the proposed configurations it is possible to decrease the maximum temperatures of the SS 316L(N)-IG launcher and receiver mirrors from by 83.5% and 89.5%, respectively.

2. Fundaments

Within the ITER tokamak, heat transfer exists in three forms: i) conduction; ii) convection and; iii) radiation.

2.1. Conduction

Conduction may be defined as the energy transfer on the form of heat in the same medium, from one point to another. The amount of heat transmitted per unit of cross-section area per unit of time, is called heat flux and may be expressed by Fourier's law as

$$q" = -k\frac{dT}{dx}, \qquad (1)$$

where k is the thermal conductivity and T is the temperature.

Thermal diffusivity α which, is the capacity that a material has to conduct thermal energy relatively to its capacity to store [5], may be expressed as

$$\alpha = \frac{k}{\rho c_p}, \qquad (2)$$

where ρ is the material density and c_p is the specific heat at constant pressure.

2.2. Convection

Convection occurs between different fluids, between fluids and surfaces or even between parts of the same fluid, provided that a temperature gradient exists.

Assuming that a surface is at temperature T_s, in contact with a fluid at temperature T_∞ and with a given convection coefficient h, the heat

flux expressed through Newton's law of cooling as [5]

$$q"_s = h(T_s - T_\infty). \quad (3)$$

In this work, forced convection in internal flow are the most relevant. Therefore, it is considered that Reynolds' number, for internal flows, may be expressed as

$$Re_D = \frac{\rho u_m D_h}{\mu} = \frac{\dot{m} D_h}{A\mu}; \quad (4)$$

$$D_h = \frac{4 * A}{P}; \quad (5)$$

where u_m is the mean flow velocity, D_h is the characteristic hydraulic diameter (see Eq. (5)), A and P are the cross-section area and perimeter, respectively, μ is the viscosity of the fluid and $\dot{m}$ is the mass flow rate.

Knowing the average inlet, $T_{m,i}$, and outlet temperatures, $T_{m,o}$, the mass flow rate and the specific heat, the power may be expressed as

$$q_{conv} = \dot{m} c_p (T_{m,o} - T_{m,i}). \quad (6)$$

The Nusselt number, defined as the quotient between the heat transferred by convection and by conduction in a fluid [5], may expressed for internal flows as

$$Nu_D = h\, D_h / k. \quad (7)$$

If the flow is considered turbulent and fully developed (where $Re_D \geq 10^3$ and Pr between 0.6 and 160) then,

$$Nu_D = 0{,}023\, Re_D^{4/5}\, Pr^n, \quad (8)$$

where n is 0.4 if $T_s > T_m$ and 0.3 if $T_s < T_m$ and T_m is the mean fluid temperature.

2.3. Radiation

Heat transfer by radiation is the only form that does not require a material medium to occur. The emissive power of a body may expressed as [5],

$$E = \varepsilon \sigma\, T_s^4\,, \quad (9)$$

where, ε the emissivity of the surface of the body and σ is the Stefan-Boltzmann constant.

If the medium is opaque, the radiative net flux may be expressed as,

$$q"_{rad} = \varepsilon \sigma T_s^4 - \alpha_{abs} G\,. \quad (10)$$

being α_{abs} the absorptivity and G the irradiation.

Considering that $\varepsilon = 1$ for black body, from Eq. (9), one obtains that its emissive power may be expressed as,

$$E_b = \sigma T^4. \quad (11)$$

From an energy balance, one can obtain that

$$\varepsilon = \alpha_{abs}. \quad (12)$$

Considering an opaque, diffuse, gray surface with incident radiation from a black body, the reflectivity may be expressed as

$$\rho_{ref} = 1 - \alpha_{abs} = 1 - \varepsilon. \quad (13)$$

To analyze the radiative exchange between two or more surfaces it is necessary to calculate view factors F_{ij}, that can then assume a value between 0 and 1. Following, are two relevant relations of the view factors:

$$A_i F_{ij} = A_j F_{ji}\,, \quad (14)$$

$$\sum_{j=1}^{N} F_{ij} = 1, \ldots, N\,, \quad (15)$$

where N is the number of surfaces [5].

The irradiation may be expressed as

$$G_i = \sum_{j=1}^{N} A_i F_{ij} J_j\,. \quad (16)$$

where J is the radiosity.

If radiation exchange occurs between a small surface at T_s and a much larger isothermal surrounding gray or black surfaces at T_{sur}, the net rate of radiation heat transfer flux may be expressed as

$$q"_{rad} = \varepsilon \sigma (T_s^4 - T_{sur}^4). \quad (17)$$

When solving radiation problems recurring to computational methods, the estimation of the view factors may be performed using the hemicube method in which, a surface of a $3D$ body that emits radiation, it is divided into N smaller $2D$ elements. Hence, the accuracy of the results depends on the resolution of the hemicube method, [6].

The microwaves present in the ITER CTS system have a density distribution on the launcher mirror that may be expressed, in Cartesian coordinates as:

$$P_{beam}(x,y) = P_{tot} \frac{2}{\pi w_x w_y} \exp\left(-2\left(\frac{x^2}{w_x^2} + \frac{y^2}{w_y^2}\right)\right), \quad (18)$$

where w_x and w_y are the characteristic dimensions of the microwave beam with a Gaussian distribution and P_{tot} is the total power of the beam [7].

For metals, the fraction of power absorbed due to a normal incidence of radiation, assuming that the transmitted fraction is negligible, may be expressed as

$$A_{abs} = \left(\frac{4}{Z_0}\right) \sqrt{\pi f_{Hz} \mu_0 \rho_{res}}, \quad (19)$$

where Z_0 and μ_0 are the empty space impedance and permeability, respectively, f_{Hz} is the gyrotron frequency and ρ_{res} is the electrical resistivity.

2.3.1. Internal Heat Generation

In this work, internal heat generation is considered as the collision of neutrons with the atoms of a body is responsible for the

generation of internal heat. This process consists in converting the kinetic energy of the neutrons into heat at the time of the shock with the atomic particles. According to [8], this heat source can be presented on the form of heat flow that may be estimated using the Monte Carlo N-Particle (MCNP) code [9].

2.4. FEM Applied to Heat Transfer

In the computational software used for the FEA, ANSYS®, are available numerous types of Finite Elements (FEs), from $1D$ to $3D$, as well as the number of nodes and degrees of freedom associated to each of these. In this work, the following FEs are used [10]: SOLID90; SHELL131, SURF152, SURF252 and FLUID116.

The thermal FEA, based in the heat transfer equation may be expressed as [6]

$$\begin{gathered}[C]\{\dot{T}\} + [K_T]\{T\} = \{R_T\} \\ [K_T] = [K_k] + [H_{conv}] + [H_{rad}] \\ \{R_T\} = \{R_B\} + \{R_{conv}\} + \{R_{h_{rad}}\} + \{R_{\dot{q}}\}\end{gathered} \quad (20)$$

where $[C]$ is the global specific heat matrix, $[K_T]$ is the global thermal conductivity matrix and $\{R_T\}$, $\{T\}$ and $\{\dot{T}\}$ are the vectors of thermal loads, temperature and first temperature derivative, respectively. Furthermore, $[K_k]$, $[H_{conv}]$ and $[H_{rad}]$ are the global matrices of conduction, convection, and radiation, and $\{R_B\}$, $\{R_{conv}\}$, $\{R_{h_{rad}}\}$ and $\{R_{\dot{q}}\}$ represent the global vectors of heat flow, convection, radiation and heat generation, respectively.

2.5. Fluid Flow

For the numerical fluid flow analyses, ANSYS®Fluent CFD software is used. It solves partially differential equations, in a control volume, based on the finite volume method and uses the SIMPLE algorithm [11].

The turbulence model implemented is the RNG k_ε model that is derived from the instantaneous Navier-Stokes equations using a mathematical technique called renormalization group methods [12].

The convective heat transfer in the k_ε models, in ANSYS®Fluent [11], is modeled using the concept of Reynolds' analogy to turbulent momentum transfer and may be expressed as

$$\frac{\partial}{\partial t}(\rho E_{tot}) + \frac{\partial}{\partial x_i}[u_i(\rho E_{tot} + p)] = \frac{\partial}{\partial x_i}\left(k_{eff}\frac{\partial T}{\partial x_i}\right) + S_h, \quad (21)$$

where E_{tot} is the total energy and k_{eff} is the effective conductivity.

To accurately treat the flow near the wall the enhanced two-equation models that combine enhanced wall treatment with the k_ε models is used [11].

2.5.1. Pressure Drop in Channels

To determine the pressure drop necessary to maintain the flow it is necessary to estimate the existing load losses.

The pressure-drop in channels may be determined by the energy equation as

$$\frac{p_1}{\rho g} + \frac{v_1^2}{2g} + z_1 = \frac{p_2}{\rho g} + \frac{v_2^2}{2g} + z_2 + h_f, \quad (22)$$

Where p_i is the pressure, v_i is the flow velocity, g is the gravitational acceleration, z_i is the height of the inlet and outlet and h_f is the head loss [13].

Local losses that may occur in channel entrance, bends, elbows and others may be expressed as

$$h_{tot} = \frac{v^2}{2g}\left(f\frac{\Delta L}{D} + \sum_i K_i\right), \quad (23)$$

where K_i is the dimensionless local loss coefficient, f is the Darcy coefficient or the friction factor, ΔL is the duct length and D is the duct characteristic diameter [13].

Hence, considering all the assumptions and equations previously presented, the following equation for the pressure drop is obtained

$$\Delta p = p_1 - p_2 = \rho g(\Delta z + h_{tot}). \quad (24)$$

With this brief introduction to the fundaments, following are described the methodologies developed and used to address the problem considered.

3. Methodology

Before proceeding to the FEA of the mirrors, two verification models (convection and radiation) are introduced to verify the implementation of the fundamental concepts, e.g., radiosity solver. The verification is conducted by comparing the numerical and analytical solutions obtained.

3.1. Verification models

The first verification model regards the study of heat transfer by convection. Consider a parallelepiped, see Figure 3 a), of length L, with a center hole of diameter D, that allows the flow of water, with an initial temperature of $T_{m,i}$ and a specific pressure, p. On one side of the parallelepiped is imposed a heat power of P while the other sides are considered adiabatic. The objective is to estimate the outlet temperature, $T_{m,o}$, of the water as well as the average hole surface temperature T_s.

The second verification model focuses on heat transfer by thermal radiation. Consider

two irradiating surfaces with temperatures, T_1 and T_2, and emissivity, ε_1 and ε_2, spaced by a

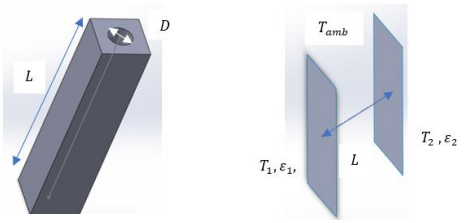

a) b)

Figure 3 - Convection a) and radiation models b).

distance L, at an environment temperature T_{amb}, see Figure 3 b).

The objective is to assess the accuracy of ANSYS® shape factor and radiosity solver calculations.

3.2. Launcher mirror

The CAD models of the launcher mirror and enclosure, see Figure 4, are developed in CATIA® accounting for the dimensions and position accessed via ENOVIA® (CAD data base).

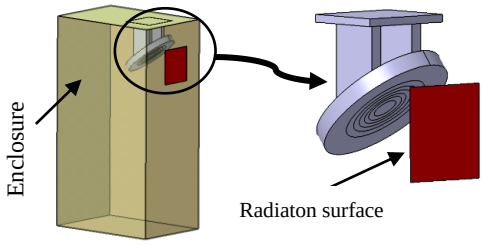

Figure 4 - CAD of launcher mirror and enclosure.

The dimensions considered are the thickness at the reflective surface lowest point (being this surface concave), of 20 mm and the mirror outline defined by an ellipse with the largest and smallest radius equal to 100.7 mm and 80 mm, respectively.

Note that the reflective surface is divided in areas, as shown in the Figure 4. These areas are necessary to enable the radiation beam power distribution implementation in ANSYS®.

Moreover, those surfaces are limited by the isolines that are computed using the methodology described next in § 3.2.1.

3.2.1. Microwaves Power Distribution

The microwave radiation from the gyrotron is incident on the launcher mirror with a distribution expressed by Eq. (18). As it represents a Gaussian power distribution on the face of the launcher mirror, the calculations of the shape of the isolines and the power between are performed using a software developed using MATLAB®.

3.2.2. Steady State Thermal FEA

Initially, a study on how to model, the plasma and stray radiation heat fluxes [14]-[15], in ANSYS® is conducted to assist in deciding if the corresponded heat fluxes may be approximated by a radiating surface, see Figure 4, at a certain temperature, emitting the correspondent thermal radiation heat flux which, minimizes the computational effort required for the analyses.

Afterwards, an initial thermal FEA of the mirror without a cooling system is conducted to verify that cooling is indeed required as the maximum temperature exceeds the operation temperature of 450℃.

To identify the most significant thermal load, it is simulated, in ANSYS®, the thermal response of the mirror to the thermal loads separately, i.e., just radiation from the plasma and then just the power absorbed due to the microwave beam being the fraction of power absorbed due to a normal incidence of radiation. Note that the nuclear heat load distribution induced by the neutrons coming from plasma and surrounding materials is considered as internal heat generation, see § 2.3.1.

Based on the assumption that a cooling system is required, 10 different cooling channel geometries, see Figure 5, are developed and FEA are conducted considering as design variables the convection area, the convection coefficients and the material volume of the mirror after the cooling channel geometries are implemented.

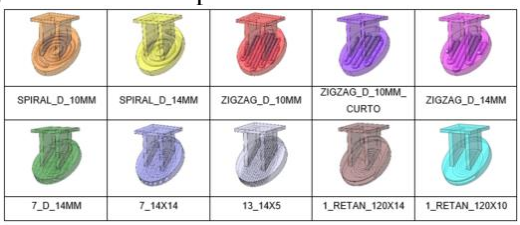

Figure 5 - CAD models of the launcher mirror with different cooling channel geometries.

For the fluid flow analysis, one further need to consider; the mass flow rate (according to [7], the maximum mass flow rate available is 1.5 $kg\ s^{-1}$ and may be used in parallel or series); the water initial temperature (~70℃) and the convection coefficient (see Eq. (8)).

As the water must always be in liquid state and knowing that the water pressure is 4.0 MPa, the maximum water temperature achieved shall not exceed 150℃, according to [16]. Additionally, the maximum pressure drop in the channels shall not exceed 1.35 MPa, as

mentioned in [17].

To assure that the pressure drop inside the channels, due to the friction losses and local losses in the elbows, are not greater than the required value of $1.35\,MPa$, simple estimations, see § 2.5.1, may be conducted in order to verify the cooling channel geometries.

3.2.3. Other Materials Considered

The methodology described above also applies to the cases in which the mirror is made of one of two other materials, i.e., copper and tungsten.

According to [18], it is considered that the material mean operation temperature for copper is between 80^0C and for tungsten is between 1000 ℃.

A performance comparison of the different channel geometries for each material is conducted. In addition, a comparison between SS 316 L(N)-IG and these two materials is performed to access their suitability as alternative materials, with respect to the maximum body temperature achieved under similar conditions.

3.2.4. Transient Thermal FEA

A transient thermal FEA is performed using one of the most adequate cooling channel geometries (according to the steady state FEA) for the SS 316L(N)-IG mirror to verify when steady state is achieved for burn (when the plasma emits radiation) and the dwell time phases. Additionally, the cooling time of the mirror during the dwell time is compared considering the cooling system turned off and turned on.

This analysis accounts for the same boundary conditions and mesh as those considered for the steady state analysis. The differences are the actuation time of the microwave beam, internal heat generation and plasma radiation, due to the dwell time phase.

3.3. Receiver Mirror

The receiver mirror is developed in CATIA® accounting for the dimensions and position accessed via ENOVIA®, see Figure 6.

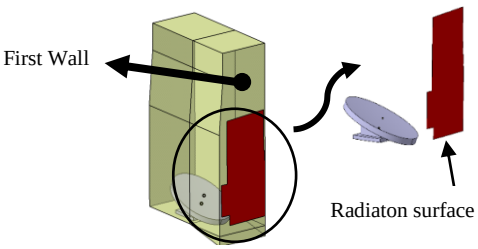

Figure 6 - CAD of receiver mirror and enclosure.

The dimensions considered are the thickness at the reflective surface lowest point (being this surface concave), of 20 mm and the mirror outline defined by an ellipse with the largest and smallest radius equal to 190 mm and 140 mm, respectively.

Similar approaches, methodologies, assumptions and simplifications are used here as those used for the launcher mirror, see § 3.2. The main difference is that the receiver mirror does not have any incident microwave beam.

3.4. Steady State Fluid Flow Thermal Analysis

A steady state fluid flow thermal analysis is performed to verify the convective coefficients used in the thermal FEA conducted. Additionally, a study related to the pressure drop inside the cooling channels, that should be lower than $1.35\,MPa$, is conducted. The results are verified with analytically calculations of the pressure drop, see § 2.5.1.

For the launcher mirror are considered cooling channel geometries ZIZAG_D_10MM and 1_RETAN_120x14 and for the receiver mirror are considered ZIZAG_D_14MM and 1_RETAN_240x14.

The turbulence model considered, see § 2.5, is the RNG k_ε model with enhanced wall treatment.

For the residuals are considered values of 10^{-6} for the energy equation and 10^{-4} for the others, e.g. the continuity equation, as indicated in [11]. Relatively to the mesh, a mesh refinement is conducted for each mirror and cooling channel geometry considering the mesh point distribution, smoothness and skewness [11]. The mesh refinement is considered satisfactory when the deviations of the results between each refinement are $< 10^{-1}$.

4. Results and Discussions

The main results obtained and respective discussion follows.

4.1. Verification Models

Using the methodology described in § 3.1 it is possible to verify that for both verification models (Convection and Radiation) the results obtained with ANSYS® are satisfactorily close to the results obtained analytically, see Table 1 and Table 2.

Table 1 - Analytical and numerical $T_{m,o}$ and T_s for the heat transfer by convection verification model.

	$T_{m,o}$ (ºC)	T_s (ºC)
Analytical	125.47	886.61
Numerical	123.69	886.34

Table 2 - Deviation between analytical and numerical results thermal radiation verification model.

	F_{ij}	E	G	q_{net}
Surface 1	~2	~0.017	~7.516	~ 0.238
Surface 2		~0.018	~14.159	~15.658

Regarding the convection model, the maximum deviation is approximately 1.4% for $T_{m,o}$. For the radiation model, the maximum deviation of 15.7% is obtained for q_{net} which is satisfactory as the analytical value of F_{ij} is visually extracted from a plot.

4.2. Launcher Mirror

4.2.1. Microwaves Power Distribution

From the methodology presented § 3.2.1, using the software routine developed in MATLAB® environment, one obtains the shape of the isolines (that are ellipses defined by its largest and smallest radius, a and b, respectively) and the power in the area delimited by two isolines, see Table 3.

Table 3 - Ellipses parameters "a" and "b" and the power beam intensity between each isoline.

Isoline	a [mm]	b [mm]	P_{tot} [KW]
1	13	14	177.5
2	26	21	138.2
3	33	26	152.3

From, Table 3 one observes that maximum power of the beam is in the center of the mirror and gradually decreases to its minimum value at the edge of the surface, as expected. Hence, the cooling system must have a higher actuation on the center area of the mirror.

4.2.2. Steady State Thermal FEA

A steady state thermal FEA is conducted, following the methodology described in § 3.2.2.

Initially, it is verified that the heat fluxes $q"_{plasma+stray} = 525\ [kWm^{-2}]$ may be approximated by a radiating surface at a T_s = 1484 [℃], see Eq. (3), emitting similar thermal radiation heat flux which, see Table 4, minimizes the computational effort required for the following analyses.

Table 4 - Incident radiation and maximum mirror temperatures.

	Incident radiation [W]	Maximum temperature [℃]
$q"_{plasma+stray}$	7273.30	2307.30
T_s = 1484 [℃]	6997.50	2306.52

To study the contribution of the different combinations of thermal loads on the maximum temperature of the launcher mirror, consider: power absorbed fraction for SS 316L(N)-IG, $A = 0.56\%$; mirror surrounding surfaces and support base temperature, 150 ℃; mirror reflective surface emissivity (polished surface), $\varepsilon_{rad} = 0.1$; other mirror surfaces emissivity (for 450 ℃), $\varepsilon_{rad} = 0.5$; internal heat generation value, $\dot{q} = 3\ [MWm^{-3}]$; surface (Figure 4 in red) temperature, T_s = 1484 ℃.

In Table 5 are presented the maximum temperatures considering the different combinations of thermal loads.

Table 5 - Maximum temperature for different combinations of thermal loads.

	T_{max}[℃]
Microwave	1765.70
Stray + Plasma Radiation	887.25
All of the above	2306.52

From Table 5, one observes that the most relevant heat load for the SS 316L(N)-IG mirror without cooling channel is the microwave beam. When considering all thermal load contributions, one verifies that a cooling system is required as the maximum mirror temperature $T_{max} = 2306.52$℃ is greater than the maximum operational temperature of 450ºC.

Following, are developed 10 different cooling channel geometries, see Figure 5.

Knowing that a cooling system is required, the channels must have an acceptable pressure drop. Hence, it is chosen the geometry, ZIGZAG_D_10MM, that apparently has the characteristics to have higher head losses as it has the highest value of ΔL (1308.9mm), due to its geometry (the highest number of 180° and 90° elbows, 9 and 2 respectively) and it has the smallest diameter ($d = 10mm$).

With this information and the Reynolds' number is possible to use the Moody diagram and obtain the value of $f = 0.03$. In addition, knowing that $R_{180°} = 7.5\ mm$ and that $R_{90°} = 10\ mm$ is possible to obtain that $K_{180°} = 0.33$ and $K_{90°} = 0.22$. Finally, with the Eq. (11) it is possible to compute the Δp, see Table 6.

Table 6 - Pressure drop for ZIGZAG_D_10MM.

Mass flow rate $[Kg/s]$	1.50	1.00	0.50	0.25
$V\ [m/s]$	19.10	12.73	6.37	3.18
Re_d	5.28E5	3.52E5	1.76E5	8.79E4
$\Delta p\ [MPa]$	1.33	0.59	0.15	0.04
$P_2\ \ [MPa]$	2.67	3.41	3.85	3.96

From Table 6, one observes that the maximum pressure drop is 1.33 MPa which, is less the maximum allowable ($1.35MPa$), meaning that there are no problems related with Δp.

The values of h, A_c and V_{water} are presented in Figure 7 and Figure 8.

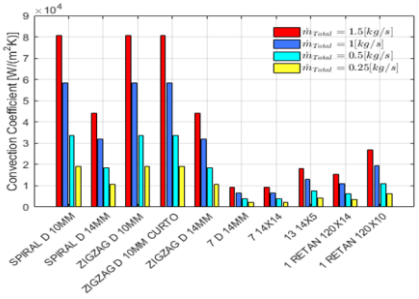

Figure 7 - Convective coefficient for the cooling channel geometries and mass flow rates considered.

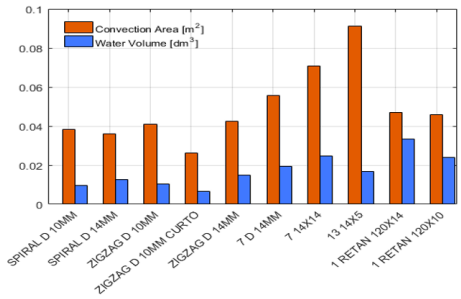

Figure 8 - Convection area and water volume for the cooling channel geometries.

Following the methodology described in § 3.2.2, the FEA are conducted for the 10 different cooling channel geometries.

The most adequate cooling channel geometry, i.e., the one that present the lowest maximum temperature, see Figure 9, is 1_RETAN_120x14.

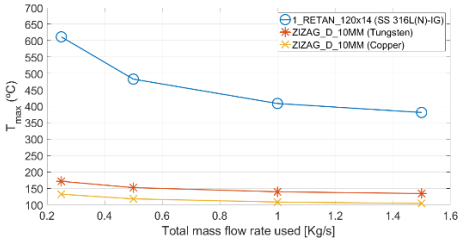

Figure 9 - Best cooling channel geometry for SS 316L(N)-IG, tungsten and copper.

Hence, one obtains a maximum temperature of 381ºC with a mass flow rate of 1.5 $kg\ s^{-1}$, considering a series fluid flow configuration.

From these steady state FEAs, one other further concludes that for SS 316L(N)-IG mirrors the most penalizing heat transfer mechanism is conduction due to the low thermal diffusivity of SS 316L(N)-IG.

To take advantage of the higher thermal diffusivity of copper and tungsten, these are considered as alternative materials for the mirror.

The results of the thermal FEAs are presented in Figure 9, from which, one obtains minimum maximum temperatures for: i) copper of $\sim 105^0C$ which, is above its operational temperature (80^0C), hence not a viable solution, and; for tungsten of $\sim 151^0C$ which is below its operational temperature (1000^0C). In contrast with the SS 316L(N)-IG, for copper and tungsten, the most relevant heat transfer mechanism is convection

4.2.3. Transient Thermal FEA

Transient thermal FEAs are conducted for 1_RETAN_120x14 following that described in § 3.2.4, for burn and dwell time phases of 400s and 1400s, respectively, considering that a mass flow rate of 1.5 $kg\ s^{-1}$ is turned on and off during the dwell time phase, see Figure 10.

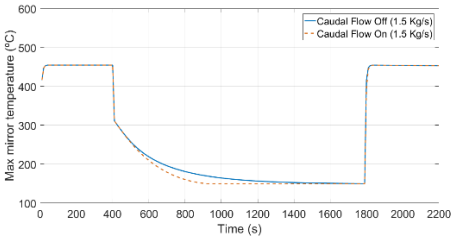

Figure 10 - Maximum mirror temperature with flow on and off during the dwell time phase.

From Figure 10, it is verified that steady state is achieved during the burn time phase. In addition, the minimum temperature (150°C) is achieved during the dwell time, even when the flow is turned off.

4.3. Receiver Mirror

The receiver mirror is analyzed according the methodology described in § 3.3, considering only four cooling channel geometries (ZIGZAG_D_10MM, ZIGZAG _D_14MM, 27_14x5 and 1_RETAN_240x14, see Figure 11) based in the tendency of being more favorable to present the highest convective coefficient, highest convective area, lowest volume of material and best combination of the three.

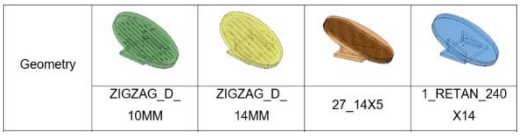

Figure 11 - Cooling channel geometries for the receiver mirror.

This tendency is obtained from the study previously conducted for the launcher mirror.

4.3.1. Steady State Thermal FEA

A steady state thermal FEA, following the methodology described in in § 3.3, is conducted obtaining a maximum temperature of 1063.80 ℃. Hence, a cooling system since is required as it is above the operational temperature of 450ºC.

The values of h, A_c and V_{water} for the 4 cooling channel geometries are presented in Figure 12 and Figure 13.

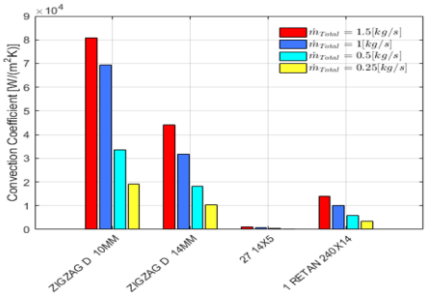

Figure 12 - Convection coefficients.

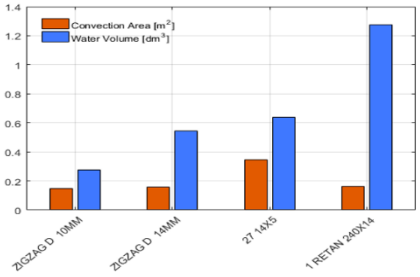

Figure 13 - Convection area and the water volume.

In Figure 14 are illustrated the maximum temperatures obtained from which, one observes that the lowest mirror temperature is achieved with the cooling channel geometry 1_RETAN_240x14 as it allows a design with less SS 316L(N)-IG.

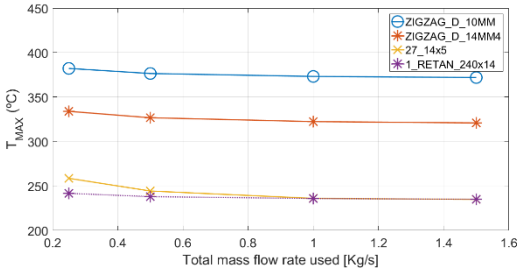

Figure 14 - Maximum mirror temperature vs total mass flow rate for different channel geometries.

However, a similar performance is achieved with 27_14x5, for higher mass flow rates, reveling that the parameters related with convection can be tuned to satisfactory results.

4.3.2. Transient Thermal FEA

From the transient thermal analysis performed for the receiver mirror one concludes that steady state is achieved during the burn time phase and the minimum temperature (150℃) is achieved during the dwell time, even when the flow is turned off.

4.4. Steady State Fluid Flow Thermal Analysis

Following the methodology described in § 3.4 the pressure drop and of h values assumed for the thermal FEA are estimated.

In Figure 15 are illustrated the local h and pressure values for the RETAN cooling channel geometries of the launcher and receiver mirrors, respectively.

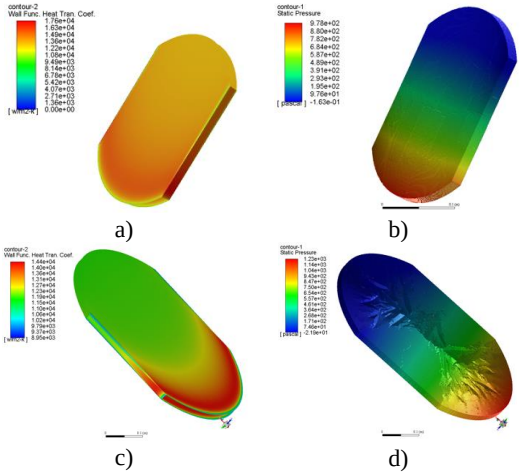

Figure 15 - RETAN mirror cooling channel geometry: a) Launcher local h; b) Launcher pressure values c) Receiver local h and; d) Receiver pressure values.

In Table 7 are presented the analytical and ANSYS®Fluent results for the RETAN_120 x14 and 1_RETAN_240x14, launcher and receiver mirrors, respectively.

Table 7 - Analytical and FLUENT results for the RETAN_120x14 and 1_RETAN_240x14, launcher and receiver mirrors, respectively.

		RETAN_120x14	RETAN_240x14
$u_m\ [m/s]$		3.04	2.73
Analytical	$\Delta p\ [MPa]$	$7.22E-3$	$1.49E-2$
	$h\ \left[\frac{W}{m^2K}\right]$	15427	14006
FLUENT	$\Delta p\ [MPa]$	$9.78E-4$	$1.23E-3$
	$h\ \left[\frac{W}{m^2K}\right]$	13663	12088

Note that the h values presented in Table 7 are the average of the local values illustrated in Figure 15 a) and c) whereas, the pressure drop are the maximum pressure values illustrated in Figure 15 b) and d).

From Table 7, one verifies that the values of the pressure drop are slightly higher than the analytical values but are still lower than the limit pressure drop of $1.35\ MPa$. Relatively to h, it is possible to verify that the analytical values are lower than those computed using ANSYS®Fluent, heat removal by convection is higher. However, recalling that for the SS 316L(N)-IG the most relevant heat transfer mechanism is conduction, see § 4.2.2 and § 4.3.1, these deviations are not significant as they do not influence the maximum temperatures obtained in the mirrors.

5. Conclusions

A study on the development of a cooling system for the launcher and receiver mirrors of the ITER CTS system is conducted as the maximum temperatures of the SS 316L(N)-IG mirrors are above the required operational temperature of 450^0C. Besides SS 316L(N)-IG, tungsten (with an operational temperature of 1210^0C) and copper (with an operational temperature of 87^0C) are also considered for the mirrors and they present relative higher thermal diffusivity.

With one of the proposed configurations it is possible to decrease the maximum temperatures of the SS 316L(N)-IG launcher and receiver mirrors from $\sim 2306^0C$ and $\sim 1064^0C$ to $\sim 381^0C$ and $\sim 240^0C$ which, corresponds to a maximum temperature decrease of 83.5% and 89.5%, respectively. Additionally, one concludes that: i) the use of copper for the mirrors is not viable as the minimum maximum temperature obtained is $\sim 105^0C$ which, is above the operational temperature of copper (87^0C) and; ii) on the other hand, the use of tungsten for the mirrors is a viable solution as one obtains a minimum maximum temperature of $\sim 151^0C$ which is below the operational temperature of tungsten (1210^0C). Even though tungsten seems to be a more adequate material for the mirrors as it presents lower maximum temperatures, the manufacturing processes of tungsten mirrors with cooling channel geometries should be further contemplated in future works.

References

[1] Song Y, Wu W, Du S (2014). *Tokamak Engineering Mechanics*. Springer Berlin Heidelberg.

[2] How Nuclear Fusion Reactors Work. Accessed on 30th August 2017 at: http://science.howstuffworks.com/fusion-reactor4.htm.

[3] Korsholm S.B. (2016). *CTS System Design Description Document. F4E_D_33NQC3.*

[4] Moseev D., Korsholm S.B., Meo F. (2011). *Fast Ion Dynamics in ASDEX Upgrade and TEXTOR Measured by Collective Thomson Scattering*. DTU.

[5] Bergman T.L., Incropera, F.P. (2011). *Fundamentals of Heat and Mass Transfer*. John Wiley & Sons.

[6] ANSYS B. (2013). ANSYS Mechanical APDL theory reference.

[7] Korsholm S.B. (2017). *Low Field Side Colletive Thomson Scattering – Load Specification*. F4E-FPA-393 SG04.

[8] Santos R., Policarpo H, et al. (2015). Material Assessment for ITER's Collective Thomson Scattering first mirror. ANIMMA.

[9] McKinney G.W, Brown F. B., et al. (2014). MCNP 6.1.1 New Features Demonstrated. IEEE 2014 Nuclear Science Symposium, LA-UR-14-23108.

[10] ANSYS, Inc. (2012). An Mechanical APDL Element Reference.

[11] Fluent, ANSYS (2013). ANSYS Fluent User's Guide.

[12] Icepak, ANSYS (2013). ANSYS Icepak User's Guide.

[13] Oliveira L.A., Lopes A.G. (2012). *Mecânica dos Fluidos*. Lidel: Lisboa.

[14] Quental P.B., Policarpo H., Luís, R., et al. (2016). Thermal Analysis of the in-vessel Components of the ITER plasma-position Reflectometry. *Review of Scientific Instruments*, *87*(11), 11E720.

[15] Silva A., Policarpo H., Varela P. (2016). *Assessment of Stray-Radiation Protection Needs for the PPR in-vessel Components.* F4E_D_24LLE8.

[16] Moran M.J., Shapiro H.N., Boettner, D.D., Bailey M.B. (2010). *Fundamentals of Engineering Thermodynamics*. John Wiley & Sons.

[17] Qinqsheng H. (2016). *Mass Flow Allotment for EQ12*. ITER_D_U3HUCQ.

[18] CES Edupak 2013 [CD-ROM]. Granta Design Limited.